

LARGE-EDDY SIMULATION OF CLOUD STREETS OVER THE EAST CHINA SEA DURING COLD-AIR OUTBREAK EVENTS

Wu-ron Hsu*, Jou-Ping Hou, Ching-Chi Wu

Department of Atmospheric Sciences, National Taiwan University, Taipei, Taiwan

Wen-Yih Sun

Department of Earth and Atmospheric Sciences, Purdue University, USA

Shou-Cheng Tcheng, Hsi-Ya Chang

National Center for High-performance Computing, Hsinchu, Taiwan

1. INTRODUCTION

Convective boundary layer develops as very cold air originated from Siberia and China breaks out over the Japan Sea, the Yellow Sea, and the East China Sea during winter seasons. The CBL quickly deepens away from the coastline of China with increasing fetch length and increasing sea surface temperature. As the depth of the CBL changes, the embedded roll vortices (cloud streets) grow in size. The convection eventually becomes three-dimensional in the farther downstream region (Agee 1987; Miura 1986; Walter 1980).

To investigate this problem through a numerical model requires huge computer resources. This is due to the nature of the problem that convections develop in a rather inhomogeneous environment with different CBL depth and sea surface temperature. Many studies use cyclic lateral boundary condition in their large-eddy simulation (LES) model (Deardorff 1980; Moeng 1986; Hsu and Sun 1991; Chlond 1992), but the cyclic condition imposes a severe limit on what LES model can do for turbulence in an inhomogeneous environment.

We have developed the National Taiwan University / Purdue mesoscale numerical model (Hsu and Sun 2001) to simulate this phenomenon with an open lateral boundary condition. The model solves a fully compressible, nonhydrostatic system of equations explicitly with a two-stage forward-backward time integration scheme. Since the numerical procedure is neutral with respect to

both sound waves and internal gravity waves, there is no need to impose any time-smoother in the model. Thus, the model results can be very accurate and numerically stable. In addition, the explicit algorithm is particularly suited for parallel computation. Our computer program is efficiently parallelized and it is suited for this very demanding problem in terms of computer resources. Furthermore, the computer program is coded in such a way that computer memory is addressed locally for all participating CPU processors in a simulation. Thus, the more CPU processors we can access in a computer job, the larger number of grid points we can have in a simulation. This will allow us to adopt a very demanding (in terms of computer resources) open lateral boundary condition in the model.

With the use of an open lateral boundary condition along the mean wind direction on both ends of the calculating domain, we are able to simulate the roll vortices under heterogeneous environment. Our preliminary results showed that the size of convection rolls indeed changes along the mean wind direction and the model reproduces all major characteristics of the CBL.

2. NATIONAL TAIWAN UNIVERSITY (NTU) / PURDUE NONHYDROSTATIC MODEL

The NTU/Purdue Nonhydrostatic Model is an extension of the Purdue Regional Model (PRM) (Chern 1994; Hsu and Sun 1994) which is a hydrostatic model. The original PRM employs a forward-backward time integrating scheme. The new nonhydrostatic model builds an additional forward-backward procedure for treating sound waves (Hsu and Sun 2001).

The vertical coordinate of the model is defined as:

* *Corresponding author address:* Wu-Ron Hsu, Dept. of Atmospheric Sciences, National Taiwan University, Taipei 106, Taiwan; e-mail: hi@webmail.as.ntu.edu.tw

$$\sigma = \frac{p_0(z) - p_0(z_{top})}{p_0(z_{surface}) - p_0(z_{top})} = \frac{p_0(z) - p_0(z_{top})}{p^*}, \quad \dots\dots\dots(1)$$

where p_0 , pressure of a reference atmosphere, is strictly a function of height. Although this vertical coordinate appears to be a σ -pressure coordinate as used in many hydrostatic models, pressure in (1) is not a function of time. The position of each grid point is fixed in time as in most of the existing nonhydrostatic models. The model employs, strictly speaking, a σ -z coordinate.

The model is three-dimensional. The governing equations are described below. Please refer to Hsu and Sun (2001) for the details of the numerical method. The momentum, mass conservation, equations are in the following formats:

$$\frac{\partial u}{\partial t} + \frac{1}{\rho} \left[\frac{\partial p'}{\partial x} + \left(\frac{\partial \sigma}{\partial x} \right)_z \frac{\partial p'}{\partial \sigma} \right] = fv - bw + Adv(u) + Diff(u), \quad \dots\dots\dots(2)$$

$$\frac{\partial v}{\partial t} + \frac{1}{\rho} \left[\frac{\partial p'}{\partial y} + \left(\frac{\partial \sigma}{\partial y} \right)_z \frac{\partial p'}{\partial \sigma} \right] = -fu + Adv(v) + Diff(v), \quad \dots\dots\dots(3)$$

$$\frac{\partial w}{\partial t} + \frac{1}{\rho} \frac{\partial \sigma}{\partial z} \frac{\partial p'}{\partial \sigma} = bu - \frac{\rho - \rho_0}{\rho} g + Adv(w) + Diff(w), \quad \dots\dots\dots(4)$$

$$\frac{\partial \rho}{\partial t} + \rho \left[\frac{\partial u}{\partial x} + \left(\frac{\partial \sigma}{\partial x} \right)_z \frac{\partial u}{\partial \sigma} + \frac{\partial v}{\partial y} + \left(\frac{\partial \sigma}{\partial y} \right)_z \frac{\partial v}{\partial \sigma} + \frac{\partial \sigma}{\partial z} \frac{\partial w}{\partial \sigma} \right] = Adv(\rho), \quad \dots\dots\dots(5)$$

where f and b are Coriolis parameters, Adv and $Diff$ represent the advection and the diffusion operator, respectively. The advection terms are calculated with Sun (1993) forward scheme. The diffusion process is parameterized through a level 2.5 turbulence scheme. Density is a prognostic variable. Pressure field is diagnosed through equation of state. The main advantage is that there is no diabatic term in the prognostic equation for density.

The current version of the model does not include ice phase of water. The equivalent potential temperature, θ_e is used as the prognostic variable in the heat equation, where θ_e is defined as:

$$\theta_e = \theta + \left(\frac{\theta}{T} \right) \frac{L_v}{c_p} q_v \quad (6)$$

Here θ is potential temperature, c_p is the specific heat at constant pressure, and q_v is specific humidity of water vapor. L_v is the latent heat of vaporization. With the definition of θ_e , the effects of latent heat due to phase change do not appear explicitly in the following prognostic equation:

$$\frac{\partial \theta_e}{\partial t} = Adv(\theta_e) + \frac{L_v q_v}{c_p} \frac{d}{dt} \left(\frac{\theta}{T} \right) + Diff(\theta_e). \quad \dots\dots\dots(7)$$

The second term on the right hand side of equation (7) takes into account the change of $\left(\frac{\theta}{T} \right)$. The prognostic equation for water in the model is:

$$\frac{\partial q_w}{\partial t} = Adv(q_w) + Diff(q_w).$$

The total specific humidity, $q_w = q_v + q_l$, is also a semi-conservative quantity in the absence of precipitation. Here q_l is the liquid water content.

We followed Deardorff (1980)'s work for the turbulence scheme with the exception that all spatial derivatives are corrected for the terrain following coordinate. Eddy-coefficient relations were employed for fluxes of semi-conservative quantities, and the sub-grid scale eddy coefficient was made proportional to the sub-grid scale turbulence kinetic energy, \bar{E} . The latter is governed by another prognostic equation not shown here. We use standard Businger et al. (1971)'s similarity theory to treat surface layer.

3. MODEL SETUP

The size of the calculating domain that we used for the simulation is 172 km by 14 km by 18 km (Fig. 1). The initial wind speed is uniform with $u = 10 \text{ m s}^{-1}$ and $v = 0$. The initial air is stable with a uniform Brunt-Väisälä frequency $N = 0.01 \text{ s}^{-1}$ and very cold (280 K) near the ocean surface. The underlying ocean is, however, quite warm with SST varies from 283 K in the left-hand-side of the domain in Fig. 1 to 290 K in the downstream region. The SST distribution will be shown in Fig. 3. Thus, we intend to simulate cold air from China (to the left of the domain in Fig. 1) encountering warmer and warmer ocean surface as it moves farther and farther away from the coastline. The cold air is also very dry, but we have imposed a relative humidity of 85% in the lower atmosphere to speed up the development

of clouds to save computer time.

Open boundary condition is imposed on both ends of the domain in the x -direction. As the cold air moves along the mean wind direction from the left, we expect that a convective boundary layer will develop. The characteristics of the air mass will be modified as it exits in the right. Thus, we imposed a realistic open lateral boundary condition in the x -direction. As for the y -direction, cyclic lateral boundary condition is sufficient as most people do for large-eddy simulations. The bottom boundary condition follows the Businger's similarity theory (Businger et al. 1971). The roughness length z_0 depends on the friction velocity of the surface layer according to Wu (1980). We used a very thick 30-level damping layer in the upper part of the domain to absorb strong gravity waves excited by convections in the lower layer.

The spatial resolution used in our simulation varies from places to places to accommodate the complicated boundary conditions efficiently. The highest resolution is used in the lowest 1 km and in the middle section of the domain along the x -direction (shaded box in Fig. 1). The grid interval in the x -direction Δx is stretched from 200 m in the interior to 2000 m on both ends of the open lateral boundaries according to a hyperbolic tangential function to avoid wave-reflection. The grid interval Δy is uniform. Δz is uniform only in the lowest 1 km ($\Delta z = 50$ m) and top 10 km ($\Delta z = 400$ m) layers and it varies in the middle levels. The time step Δt is only 0.07 s due to the explicit nature of our model. The total number of grid points is approximately 4 million points (400 by 140 by 70). The simulation is executed on an IBM Power 4 computer in the National Center for High-performance Computing in Taiwan using 16 CPU's. The total CPU time is approximately 1 day for 2 h simulation.

4. RESULTS AND DISCUSSIONS

After 2 h of simulation, a CBL developed. The structure of the CBL is best illustrated by the average virtual potential temperature θ_v cross-section over the y -direction (Fig. 2). The bottom 100 to 150 m layer above the ocean surface is the super adiabatic layer, since the SST is considerably higher than the air temperature. The mixed layer lies just above the thin super adiabatic layer with a very small vertical gradient of θ_v due to strong mixing inside the CBL. Clouds developed in the upper part of the CBL (Fig. 2) and θ_v increases slightly with height following a moist adiabatic process. The cloud top also

matches the CBL top where the vertical gradient of θ_v changes abruptly in height.

The simulated CBL becomes deeper as the cold air moves downstream absorbing heat and moisture from the warm ocean. The depth is around 500 m to the left of $x = 65$ km in Fig. 2 and quickly reaches 1200 m at $x = 85$ km. The sudden increase in CBL depth is apparently associated with the development of convective rolls (cloud streets in Fig. 3) in the area. The tips of cloud streets first appeared at $z = 300$ m level and the clouds lift upward and become thicker following the airflow. There are 14 bands of clouds within the 14 km domain in the y -direction. Thus, the aspect ratio of the roll convection is around 2:1 to 1:1. The roll convections are very strong with vertical motion reaching 2 m s^{-1} (not shown). These rolls transport a huge amount of heat and moisture into the CBL resulting in the sudden change in CBL depth. It is interesting to note that since the roll convections orient along the mean wind direction, the average over the y -direction effectively smoothes out all signals of roll convections. Thus, the average θ_v and q_i in Fig. 2 is very smooth in this part of the domain.

In the farther downstream region with $x > 85$ km, the CBL become even thicker to about 1400 m. Convections become three-dimensional (Fig. 3). The θ_v distribution in Fig. 2 is quite chaotic because the average is taken only in the y -direction for the downstream region. Figure 4 shows the horizontal cross-section of vertical velocity near the water surface at $z = 50$ m level. The areas with upward motion matches the locations with clouds as expected. The horizontal scale of the convections also become larger as the CBL become deeper and the cells appear to be 'open' with downward motion found in the cell center surrounded by narrow bands with upward motion (Fig. 4). The results seem to be quite consistent with clouds pattern seen in a visible satellite picture during a wintertime cold air outbreak event over the East China Sea.

Figures 5 and 6 show the vertical profiles of θ_v and u averaged over three horizontal areas from $x = 60$ to 70 km, 80 to 90 km and 100 to 110 km. These three areas correspond to an upstream region where cloud streets start to develop, a transition region where cloud streets changed into 3 D structure, and a downstream region with cellular cloud pattern. Our model is able to capture the major features of the CBL as the two figures have shown. Since the turbulence in the upstream area is not as strong as the other two areas, horizontal momentum u is not well mixed and the vertical wind shear is therefore larger in the upstream area. This condition is

favorable for forming cloud streets (Miura 1986). As the CBL become thicker in the downstream region, the vertical wind shear is small and 3 D cells appear.

5. CONCLUDING REMARKS

Our work is only preliminary. At the present time we have not yet included Coriolis force, large scale subsidence and radiation in the simulation. We will examine these important processes in the near future and will be able to better understand this important phenomenon.

ACKNOWLEDGEMENT

This work is sponsored by the National Science Council in Taiwan.

REFERENCES:

- Agee, E. M., 1987: Meso-scale cellular convection over the oceans. *Dyn. Atmos. Ocean.* **10**, 317-341.
- Businger, J. A., J. C. Wyngaard, Y. Izumi and E. F. Bradley, 1971: Flux-profile relationships in the atmospheric surface layer. *J. Atmos. Sci.*, **28**, 181-189.
- Chern, J. D., 1994: *Numerical simulations of cyclogenesis over the western United States*, Ph. D. Thesis, Department of Earth and Atmospheric Sciences, Purdue University, 178 pp.
- Chlond, A., 1992: Three-dimensional simulation of cloud street development during a cold air outbreak. *Boundary-Layer Meteorol.*, **58**, 161-200.
- Deardorff, J. W., 1980: Stratocumulus-capped mixed layers derived from a three-dimensional model. *Boundary-Layer Meteorol.*, **18**, 495-527.
- Hsu, W. R., and W. Y. Sun, 1991: Numerical study of mesoscale cellular convection. *Boundary-layer Meteorol.*, **57**, 167-186.
- Hsu, W. R., and W. Y. Sun, 1994: A numerical study of a low-level jet and its accompanying secondary circulation in a Mei-Yu system. *Mon. Wea. Rev.*, **122**, 324-340.
- Hsu, W. R., and W. Y. Sun, 2001: A time-split, forward-backward numerical model for solving a nonhydrostatic and compressible system of equations. *Tellus*, **53A**, 279-299.
- Miura, Y., 1986: Aspect ratios of longitudinal rolls and convection cells observed during cold air outbreaks. *J. Atmos. Sci.*, **43**, 26-39.
- Moeng, C. H., 1986: Large-eddy simulation of a stratus-topped boundary layer, 1, Structure and budget. *J. Atmos. Sci.*, **43**, 2886-2900.
- Sun, W. Y., 1993: Numerical experiments for advection equation. *J. of Comput. Phys.*, **108**, 264-271.
- Walter, B. A., 1980: Wintertime observations of roll clouds over the Bering Sea. *Mon. Wea. Rev.*, **108**, 2024-2031.
- Wu, J., 1980: Wind-Stress Coefficients over Sea Surface near Neutral Conditions - A Revisit. *J. of Phys. Oceanogr.*, **10**, 727-740.

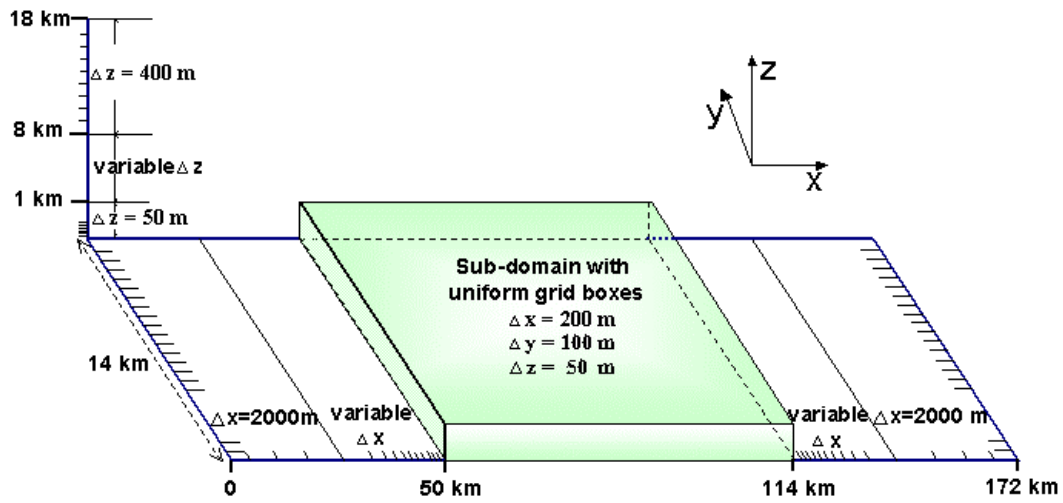


FIG. 1. Model grid point structure. The grid interval in the x -direction is stretched from 200 m in the interior to 2000 m on both ends of the open lateral boundaries. Lateral boundaries in the y -direction are cyclic with uniform Δy throughout the whole domain. Grid distance in z is also stretched as shown. The shaded sub-domain in the figure has uniform grid intervals. There are a total of 400 by 140 by 70 grid points. Note that the scales in y and z directions are exaggerated.

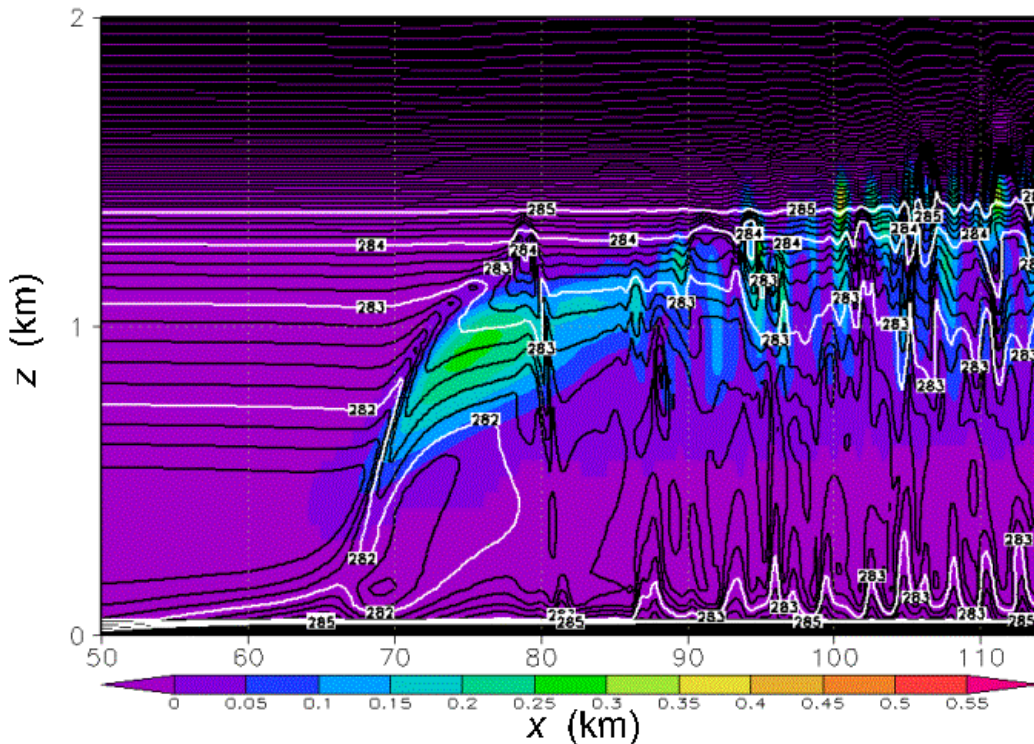


FIG. 2. Vertical cross-section of the average virtual potential temperature θ_v (with contour interval of 0.2 K), and average liquid water content q_l (color levels shown in the bottom; units in g kg^{-1}) after 2 h of simulation. The average is taken in the y -direction for the whole domain. Only the result from $x = 50$ km to 114 km is shown.

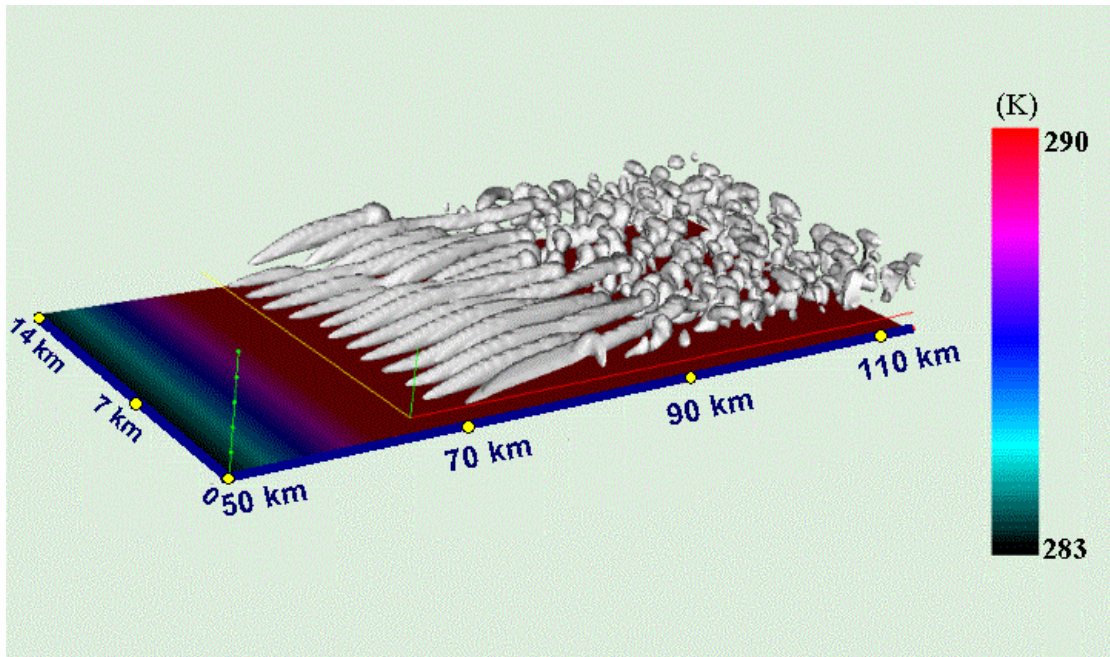


FIG. 3. The sea surface temperature (color levels shown to the right; units in K) and cloud distribution after 2 h of simulation. Grid points with liquid water content q_l greater than 0.0005 are enclosed. The thin red and orange lines identify the lowest cloud level at $z = 300$ m. Cold air enters the calculating domain from the left with mean wind $u = 10 \text{ m s}^{-1}$.

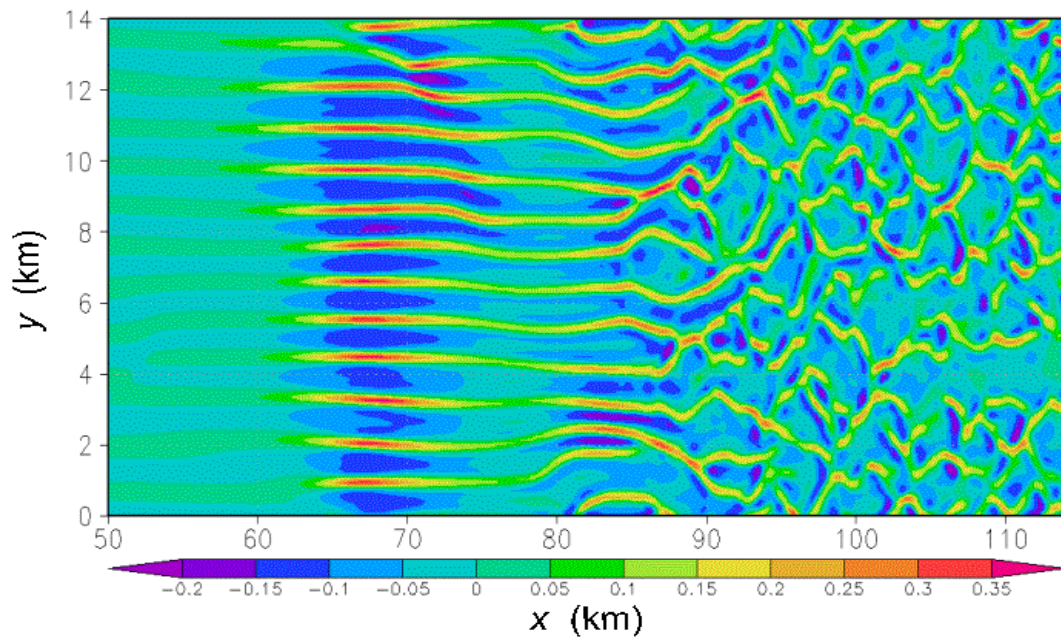


FIG. 4. Vertical velocity w at $z = 50$ m level after 2 h of simulation. Color level is shown in the bottom with units in m s^{-1} .

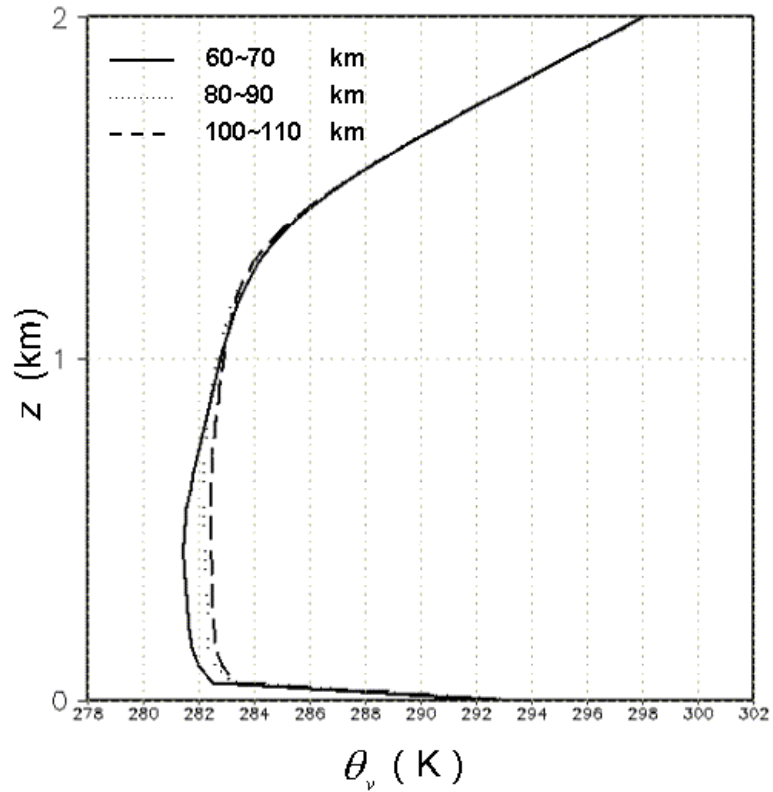


FIG. 5. Horizontal average vertical profiles of virtual potential temperature θ_v after 2 h of simulation. The average is taken in the y-direction and from $x = 60$ to 70 km (solid line); from $x = 80$ to 90 km (dotted line); from $x = 100$ to 110 km (dashed line).

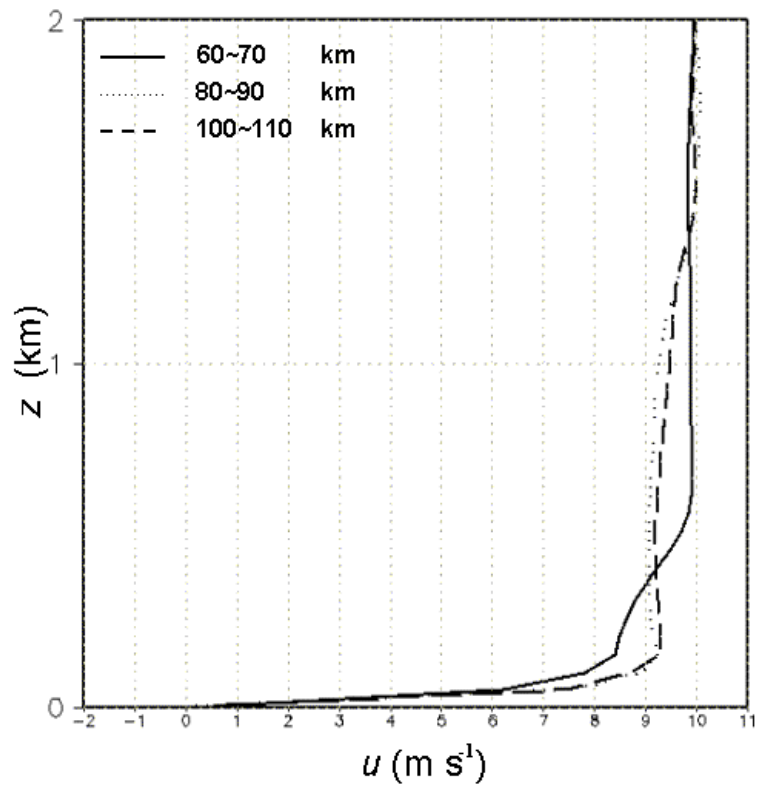


FIG. 6. Same as FIG. 5, except for u .